

SpotFormer: Multi-Scale Spatio-Temporal Transformer for Facial Expression Spotting

Yicheng Deng, *Student Member, IEEE*, Hideaki Hayashi, *Member, IEEE*,
and Hajime Nagahara, *Member, IEEE*

Abstract—Facial expression spotting, identifying periods where facial expressions occur in a video, is a significant yet challenging task in facial expression analysis. The issues of irrelevant facial movements and the challenge of detecting subtle motions in micro-expressions remain unresolved, hindering accurate expression spotting. In this paper, we propose an efficient framework for facial expression spotting. First, we propose a Sliding Window-based Multi-Resolution Optical flow (SW-MRO) feature, which calculates multi-resolution optical flow of the input image sequence within compact sliding windows. The window length is tailored to perceive complete micro-expressions and distinguish between general macro- and micro-expressions. SW-MRO can effectively reveal subtle motions while avoiding severe head movement problems. Second, we propose SpotFormer, a multi-scale spatio-temporal Transformer that simultaneously encodes spatio-temporal relationships of the SW-MRO features for accurate frame-level probability estimation. In SpotFormer, our proposed Facial Local Graph Pooling (FLGP) and convolutional layers are applied for multi-scale spatio-temporal feature extraction. We show the validity of the architecture of SpotFormer by comparing it with several model variants. Third, we introduce supervised contrastive learning into SpotFormer to enhance the discriminability between different types of expressions. Extensive experiments on SAMM-LV and CAS(ME)² show that our method outperforms state-of-the-art models, particularly in micro-expression spotting.

Index Terms—Facial expression spotting, Spatio-temporal transformer, Multi-scale feature learning, Micro-expression.

1 INTRODUCTION

FACIAL expressions are a fundamental aspect of nonverbal communication and play a crucial role in conveying human emotions. As people experience emotional changes, facial muscles undergo voluntary or involuntary movements, resulting in various expressions. These expressions act as powerful and direct social signals, enabling others to understand their emotions and enhancing interpersonal communication.

Facial expressions can be broadly categorized into two groups: macro-expressions (MaEs) and micro-expressions (MEs). MaEs typically last from 0.5 to 4.0 seconds [1] and are easily perceived by people due to their occurrence on a large facial area and high intensity [2]. The analysis of MaEs is significant in various practical applications, such as sociable robots [3], mental health [4], and virtual reality [5]. In contrast, MEs generally last for less than 0.5 seconds [6], and their perception is much more challenging due to their localized occurrence and low intensity [7]. Because of their involuntary nature, MEs are crucial in situations where people may attempt to conceal emotions or deceive others, such as in lie detection [8], medical care [9], and national security [10]. Therefore, both MaE and ME analysis play important roles in understanding human emotions and

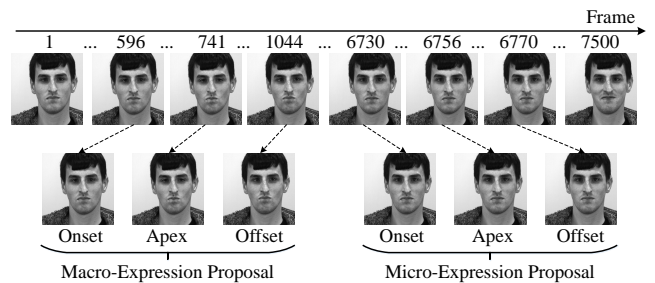


Fig. 1. Illustration of macro- and micro-expression spotting.

behaviors.

Facial expression analysis generally consists of two steps: facial expression spotting (FES) and facial expression recognition. As the initial phase, FES aims to locate the onset and offset frames of MaE and ME intervals within video sequences, as illustrated in Fig. 1. The onset frame represents the beginning of an expression, while the offset frame indicates its end. However, FES is highly challenging due to several factors, including the difficulty in detecting subtle motions that exist in MEs, the presence of irrelevant motions (e.g., head movements and eye blinking) in long videos, and the difficulty of distinguishing between MaEs, MEs, and neutral expressions.

In recent years, researchers have made significant progress in developing efficient algorithms for FES. Early studies employed traditional methods to extract hand-crafted features, such as optical flow in large sliding windows. Subsequently, they analyzed feature variations and

• Y. Deng is with the Graduate School of Information Science and Technology, Osaka University, Suita, 565-0871, Japan. Email: yicheng@is.ids.osaka-u.ac.jp

• H. Hayashi and H. Nagahara are with the Institute for Datability Science, Osaka University, Suita, 565-0871, Japan. Email: hayashi@ids.osaka-u.ac.jp; nagahara@ids.osaka-u.ac.jp

Manuscript received April 19, 2005; revised August 26, 2015. (Corresponding author: Yicheng Deng.)

detected expression intervals using threshold strategies [11], [12], [13], [14]. More recently, with the development of deep learning, more and more researchers introduced learning-based methods to address the problem [15], [16], [17], [18]. Additionally, due to the similarity between FES and temporal action localization (TAL), some researchers applied classical TAL frameworks to FES [19], [20] and introduced additional modules. These methods have achieved considerable improvements in MaE spotting performance.

Despite significant progress made by previous studies, there are still some open questions that require exploration for further performance improvement, especially for ME spotting. The first question is how to extract more robust motion features. Traditional methods typically employ a large sliding window strategy to extract optical flow features and spot potential expression proposals within each sliding window [12], [21]. However, the accuracy of using such a strategy is significantly impacted by head movement issues. In contrast, recent deep learning-based methods calculate optical flow between adjacent frames as motion features [22], [23]. Unfortunately, such an optical flow extraction method fails to effectively reveal subtle motions present in MEs. Therefore, there is an urgent need to develop a strategy that can magnify motion information while mitigating the influence of head movement. Second, some methods [19], [20] applied general TAL frameworks to FES. However, these methods overlook task-specific characteristics, such as the extremely short length of MEs and the problem of irrelevant facial movements. Additionally, they usually employ a pre-trained I3D [24] network to extract features from snippets based on the optical flow extracted between adjacent frames, which is unsuitable for revealing subtle motions as we mentioned. Consequently, their performance, particularly in ME spotting, requires improvement. Third, some methods compute optical flow in specific regions of interest (ROIs) where facial expressions frequently happen to alleviate the influence of irrelevant motions. They then design a network to learn the extracted motion features [18], [23]. However, their proposed networks need a comprehensive consideration of spatio-temporal relationships and multi-scale feature learning. This limitation restricts the representational capacity of their models.

To address the issues mentioned above, we propose an efficient framework for facial expression spotting in untrimmed videos. First, we propose a *sliding window-based multi-resolution optical flow* (SW-MRO) feature to amplify motion information while mitigating significant head movement problems. The temporal sliding window size is tailored to perceive complete subtle MEs and discern the differences between general MEs and MaEs, enabling our framework to achieve accurate frame-level apex or boundary (onset or offset) probability estimation and expression type classification. Second, we propose SpotFormer, a multi-scale spatio-temporal transformer to capture multi-scale spatial relationships and temporal variations among different facial parts across frames from the SW-MRO features. In SpotFormer, a *facial local graph pooling* (FLGP) operation is designed to extract multi-scale facial spatial features and learning-based temporal downsampling is employed to extract multi-scale temporal features, enhancing the model's understanding ability from low-level to high-level. The ex-

ploration of several model variants and extensive comparative experiments validate the effectiveness of SpotFormer. Third, we introduce supervised contrastive learning into our model to learn a finer discriminative feature representation for more effective differentiation of various expression types in long videos. This contrastive learning approach mitigates the difficulty in recognizing the boundary to distinguish between specific MaEs.

This paper is an extension of our prior conference publication [25]. The most crucial update is the proposal of SpotFormer. As other differences from the conference paper version, we make a more extensive overview and comparison of the related literature, particularly with regard to TAL. In addition, we present a more comprehensive qualitative and quantitative comparison to previous work in the experimental section. The contributions are listed as follows, where * represents new contributions of this paper:

- We propose SW-MRO, a sliding window-based multi-resolution optical flow feature for facial expression spotting, which can magnify the motion information while avoiding severe head movement problems. Extensive ablation studies demonstrate that such an optical flow feature can assist the model not only in perceiving complete subtle MEs but also in discerning the differences between general MaEs and MEs.
- * We present SpotFormer, a novel Transformer-based framework to capture spatial relationships and temporal variations at multiple scales for accurate frame-level probability estimation. In SpotFormer, a facial local graph pooling operation suitable for facial graph structure is proposed for multi-scale spatial feature learning. Extensive comparative experiments on various model architectures and multi-scale feature fusion methods verify the effectiveness of SpotFormer.
- We introduce supervised contrastive loss to our model for discriminative feature representation learning. To the best of our knowledge, our work is the first to study contrastive learning for facial expression spotting, achieving better recognition of boundaries between different types of expressions.

2 RELATED WORK

2.1 Facial Expression Spotting

In general, FES methods fall into two categories: traditional methods and deep learning methods. Early methods extracted appearance-based features, such as local binary patterns [26] and histogram of oriented gradients [27]. These methods then employed machine learning algorithms for feature difference analysis and utilized threshold strategies for expression spotting. Subsequently, the mainstream approach for motion feature extraction shifted to optical flow. He et al. [12] employed main directional maximal difference analysis [28] to detect facial movements and spot potential expression proposals based on the maximal difference in magnitude along the main direction of optical flow features. He [13] alleviated head movement problems by repeating face alignment using optical flow in the nose tip region.

Guo et al. [21] converted optical flow vectors into a polar coordinate representation and introduced a novel decision criterion based on both magnitude and angle information.

With the development of deep learning, an increasing number of researchers have proposed various neural networks for feature learning. Zhang et al. [29] employed convolutional neural networks (CNNs) to extract features from video clips and spotted apex frames by analyzing the feature representations. Verburg et al. [15] extracted histogram of oriented optical flow features to encode the temporal changes in selected facial regions. Then they employed an RNN to spot intervals likely to contain relevant facial movements. Liong et al. [30] introduced a three-stream CNN and employed pseudo-labeling techniques to facilitate the learning process. Yang et al. [31] incorporated facial action unit information and concatenated various types of neural networks for feature learning. Leng et al. [23] extracted several ROIs and adopted the main directional mean optical flow (MDMO) algorithm [32] to compute optical flow between adjacent frames. Then they utilized one-dimensional CNNs to learn temporal variations and estimate the probability of each frame belonging to an apex or boundary frame. Based on [23], Yin et al. [18] learned spatial relations by adding a graph convolutional network (GCN) to embed action unit (AU) label information into the extracted optical flow. Guo et al. [20] proposed a multi-scale local transformer, similar to ActionFormer [33], and considered multi-scale temporal feature fusion for performance improvement. Yu et al. [19] applied A2Net [34] to facial expression spotting and improved it by introducing attention modules. While current optical flow-based methods have significantly improved MaE spotting, their performance in ME spotting remains considerably lower. This is attributed to their extracted optical flow features, which cannot efficiently reveal subtle motions that exist in MEs. To solve this issue, we propose to extract a sliding window-based multi-resolution optical flow feature, which can effectively magnify these subtle motions and enhance the distinction between MaEs and MEs, thereby achieving accurate frame-level probability estimation and improving MaE and ME spotting performance.

2.2 Temporal Action Localization

Similar to FES, TAL aims to detect action intervals in general scene videos. Deep learning-based methods for TAL can be divided into anchor-based methods and anchor-free methods, with the latter further divided into frame-level probability estimation methods and boundary regression-based methods.

Early works treated TAL as a 1D object detection task. Xu et al. [35] proposed a region convolutional 3D network to encode the video streams and locate the action proposals using an anchor-based method. Chao et al. [36] refined the faster R-CNN object detection framework to make it suitable for TAL, employing a multi-scale architecture to accommodate extreme variations in action duration. However, anchor-based methods have some drawbacks. First, they require pre-defining a fixed number of anchors, resulting in increased computation and memory requirements. Second, the length and number of anchors need careful pre-

definition, limiting flexibility and affecting the generalization ability of the proposed model.

In 2018, Lin et al. [37] proposed a Boundary-Sensitive Network (BSN), pioneering a method that first locates temporal boundaries with high probabilities and then aggregates these probabilities to generate action proposals. This is the first frame-level probability estimation method, and it then became the mainstream. Subsequently, Lin et al. [38] refined BSN [37] by proposing a boundary-matching network, incorporating a boundary-matching mechanism to evaluate confidence scores of densely distributed proposals. Zhao et al. [39] argued that frame-level probability-based methods had a limited understanding of the temporal dimension, leading to inconsistency and discontinuity. They addressed this issue by proposing two consistency losses to mutually regularize the learning process. Recently, researchers have focused on refining proposals generated by previous methods. Zhu et al. [40] refined proposals generated by BSN [37] by introducing a ContextLoc, which models the local context, global context, and context-aware inter-proposal relations in a unified framework. Nag et al. [41] presented a novel Gaussian aware post-processing method for more accurate model inference, which models the start and end points of action instances with a Gaussian distribution to enable temporal boundary inference at a sub-snippet level.

Yang et al. [34] were the first to directly regress the boundary offset for each temporal point, which solves the inflexibility and computation problems of anchor-based methods. Zhang et al. presented ActionFormer [33], a simple yet effective multi-scale transformer designed to further improve action localization performance. Shao et al. [42] proposed an action sensitivity learning framework, which aims to assess the value of each frame and leverage the generated action sensitivity to recalibrate the training procedure.

Even though there are many similarities between TAL and FES, there are still some differences that make the direct application of TAL methods into FES inappropriate. The main differences can be summarized in three aspects. Firstly, motion information is usually obvious to detect in TAL videos, while in FES, the main challenge is to capture the subtle motion of MEs and suppress noises such as head movement and eye blinking. Since anchor-based methods and boundary regression-based methods typically require a large receptive field, as discussed before, extracting delicate optical flow becomes challenging. Therefore, in this paper, we design a frame-level probability-based framework.

Secondly, the scene usually changes in TAL videos, and the main challenge is to distinguish between the action scene and background change. In contrast, the scene during the whole video does not change much in FES, making it easier to capture vital motion information in certain facial areas that are strongly related to facial expressions. Therefore, in this paper, we propose a graph-based method to efficiently extract motion features while suppressing noises.

Finally, TAL involves an action classification task for each proposal since their videos may involve hundreds of action classes. However, there are only two action classes (i.e., MaE and ME) in FES. Rather than focusing on action recognition, we aim to distinguish between MEs and MaEs. Therefore, in this paper, we emphasize perceiving MEs and

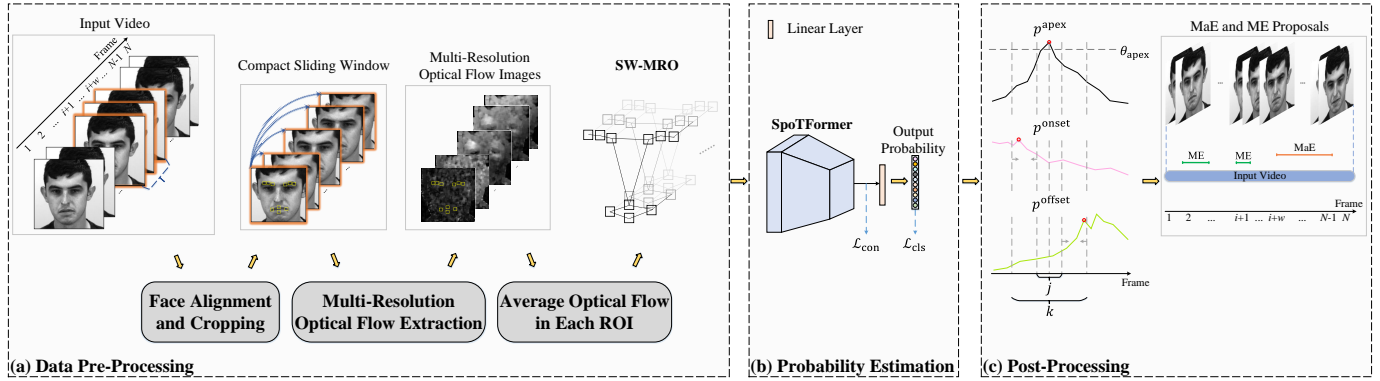


Fig. 2. Overview of the proposed framework. (a) The data pre-processing module calculates the SW-MRO features; (b) the probability estimation module employs SpotFormer which takes optical flow features as input for frame-level apex or boundary probability estimation; (c) the post-processing module aggregates the probability maps from all frames and generates expression proposals.

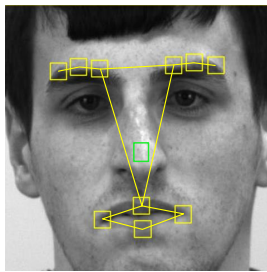


Fig. 3. Extracted ROIs and constructed facial graph structure are denoted in yellow, while the nose tip region for face alignment is denoted in green. Note that the edge connections are only for presentation, they are not involved in the model.

analyzing the differences between MEs and MaEs within compact sliding windows.

2.3 Transformer

The Transformer was first proposed by Vaswani et al. [43] for natural language processing. In recent years, many researchers have explored the Transformer for computer vision and have shown great success in 2D image processing (e.g., ViT [44], Swin Transformer [45]) and 3D video understanding (e.g., ViViT [46], Video Swin Transformer [47], ActionFormer [33]). Such success is attributed to their powerful self-attention mechanism and ability to model long-range relations. The self-attention mechanism allows the model to focus on critical features and ignore irrelevant information, enhancing performance and robustness. The long-range relation modeling enables efficient capture of context information across both spatial and temporal dimensions, contributing to a better understanding of the overall sequence. In this paper, we explore the potential of the graph-based Transformer for facial expression spotting and introduce SpotFormer, a novel model designed to enhance the accuracy of expression spotting.

2.4 Contrastive learning

In recent years, contrastive learning has proven to be effective in various domains, including computer vision and

natural language processing. The objective of contrastive learning in unsupervised learning [48] is to acquire discriminative representations by maximizing the similarity between similar instances (positive pairs generated using data augmentation) while minimizing the similarity between dissimilar instances (negative pairs). This approach produces meaningful visual representations applicable to tasks such as image recognition, representation learning, and semantic understanding. Based on the idea that positive pairs can also be selected by ground-truth labels, Khosla et al. [49] introduced the supervised contrastive loss, showcasing its potential to enhance supervised tasks by incorporating labeled information during the training process. Supervised contrastive learning efficiently enlarges the domain discrepancy, leading to an enhanced extraction of discriminative feature representations. Our method focuses on recognizing the boundary between different types of expressions. To achieve this objective, we establish contrasts between MaE and ME frames, as well as between ME frames and neutral frames. This approach enables our model to acquire more discriminative feature representations, ultimately reducing the misclassification rate.

3 PROPOSED EXPRESSION SPOTTING FRAMEWORK

An overview of the proposed framework is shown in Fig. 2. Given a raw video as input, the proposed framework aims to detect all potential MaE and ME intervals within the video, spotting the onset and offset frames, as well as assigning the expression type for each interval. The framework consists of three modules: the data pre-processing module, the probability estimation module, and the post-processing module.

3.1 Data pre-processing

Assuming that a video $V = (v_i)_{i=1}^N$ with N frames, we initially calculate the SW-MRO features. Specifically, by setting a window length w , we pad the beginning and end of the video with $\lfloor \frac{w}{2} \rfloor$ repetitions of the first and end frames, respectively. Then, we divide the entire video into N overlapped clips $C = (c_i)_{i=1}^N$ with the window length

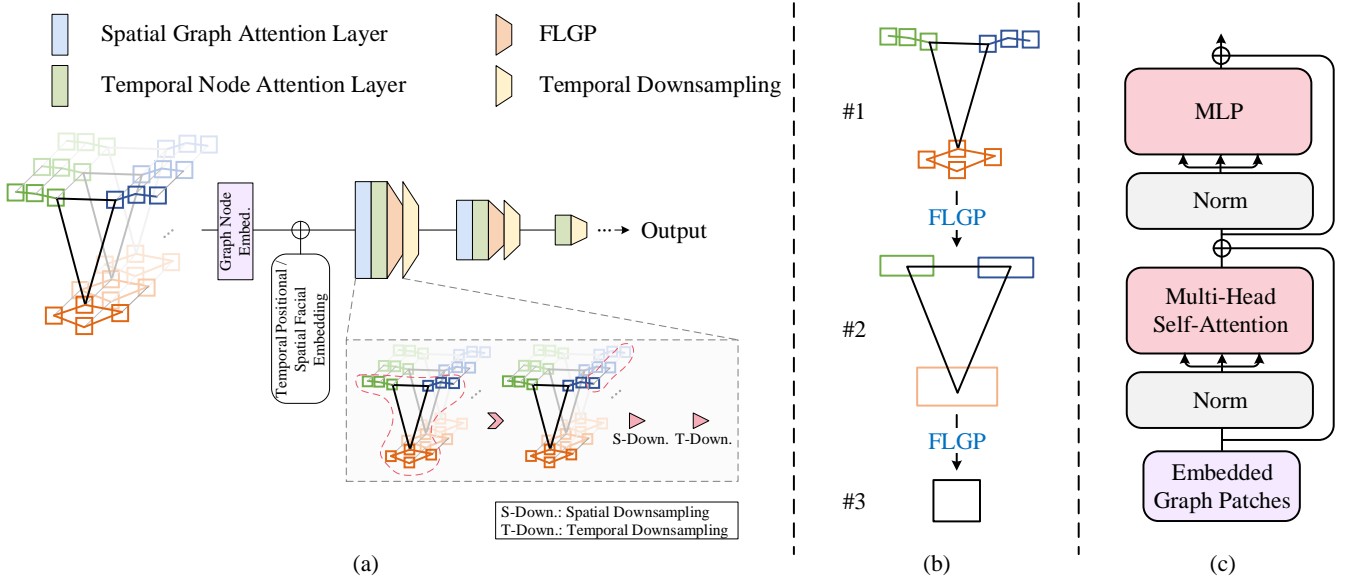


Fig. 4. Overview of the proposed SpotFormer. (a) The network structure of SpotFormer; (b) the scale change between different facial graph structures through FLGP; (c) the illustration of the spatial graph attention layer and temporal node attention layer.

w and sliding stride 1, where c_i involves v_i as the center frame. In this paper, we aim to achieve accurate frame-level probability estimation based on compact sliding windows. Specifically, we utilize all the temporal information of c_i and magnify the motion information existing in c_i to estimate the probability map of v_i . Next, we will introduce the process of obtaining multi-resolution optical flow features in each compact sliding window.

For each clip c_i , we initially detect the 68 facial keypoints using a pre-trained MobileFaceNet [50] in the first frame c_i^1 , which are then utilized for face cropping, extracting the nose tip area for face alignment, and extracting ROIs. Specifically, we detect the facial bounding box in the first frame c_i^1 . In each subsequent frame c_i^s , where $s = 2, 3, \dots, w$, we initialize the facial bounding box with the one from c_i^1 . Given that the nose tip area remains stationary during expressions [13], we compute the optical flow of the nose tip area, as illustrated in Fig. 3, to represent global head movement. Subsequently, we adjust the facial bounding box for c_i^s accordingly. To achieve this, we employ the Farneback algorithm [51] to compute MDMO optical flow [32] of the nose tip area $o_i^{s, \text{nose}} \in \mathbb{R}^2$ between c_i^1 and c_i^s :

$$o_i^{s, \text{nose}} = \frac{1}{m_i^{\text{nose}} \times n_i^{\text{nose}}} \sum_{(x, y) \in M_i^{\text{nose}}} \text{OF}(c_i^1, c_i^s)[x, y], \quad (1)$$

where m_i^{nose} and n_i^{nose} represent the height and width of the extracted nose tip area M_i^{nose} , and $\text{OF}(\cdot, \cdot)[x, y]$ denotes the value of MDMO optical flow features at (x, y) coordinates.

Based on the discussion in Sections 1 and 2, we selectively extract R ROIs, where facial expressions happen most frequently, rather than processing entire images. This choice can effectively mitigate the impact of noise and irrelevant facial movements. Then, we compute the optical flow for the selected R ROIs between c_i^1 and c_i^s to obtain MDMO optical flow features $o_i^s = [o_i^{s, r}]_{r=1}^R \in \mathbb{R}^{R \times 2}$. The computation

is similar to (1). Afterwards, we concatenate the optical flow $[o_i^1, o_i^2, \dots, o_i^w]$ to construct finer optical flow features $o_i \in \mathbb{R}^{w \times R \times 2}$ for c_i , where $o_i^1 = \mathbf{0}$. As a result of the data pre-processing, we obtain the optical flow features $O = (o_i)_{i=1}^N \in \mathbb{R}^{N \times w \times R \times 2}$ for the entire input video.

3.2 SpotFormer for probability estimation

The overview of the proposed SpotFormer is outlined in Fig. 4. After obtaining the optical flow features, the SpotFormer calculates the probabilities required for expression spotting. These include the probabilities of occurrence for onset, apex, offset, expression, and neutral states in both ME and MaE spotting. SpotFormer consists of graph node embedding, temporal positional embedding, spatial facial embedding, and multi-scale spatio-temporal attention block, aiming to comprehensively learn both spatial relations and temporal variations for accurate estimation of the probability map of every single frame. Subsequently, we will introduce each component in detail.

3.2.1 Graph node embedding

Given an input clip of optical flow features $o_i \in \mathbb{R}^{w \times R \times 2}$ for evaluating the frame v_i , we treat each graph node as a patch and use a trainable linear projection to embed each patch into D dimensions.

3.2.2 Temporal positional embedding

For the temporal dimension, following [44], we set tokens with learnable parameters, denoted as $\delta_t \in \mathbb{R}^{w \times D}$, to retain temporal positional information. Note that all graph patches in a single frame share the same temporal positional embedding.

3.2.3 Spatial facial embedding

Unlike other graph-based tasks where there are predefined edge connections among graph nodes, facial expression analysis involves many possible edge connections among different facial muscles. To mitigate the impact of these various sophisticated edge connections, SpotFormer does not explicitly consider the edges but focuses on the facial part type of each graph node instead. Inspired by [52], we introduce learnable facial part tokens to the graph nodes. Specifically, we set three tokens with learnable parameters $\delta_s \in \mathbb{R}^{3 \times D}$ for three asymmetric facial parts (left eyebrow, right eyebrow, and mouth) since MEs are asymmetric. Graph nodes belonging to the same facial part share the same facial part token. This method enables the model to understand the overall spatial facial structure without the requirement of exploring complex edge connections.

3.2.4 Spatio-temporal attention

In the spatial graph attention layer, our objective is to model the spatial correlations among all graph nodes in each frame. As shown in Fig. 4 (c), the computation of each spatial graph attention layer can be described as follows:

$$\begin{aligned} z^l &= \text{MHSA}(\text{BN}(z^{l-1})) + z^{l-1}, \\ z^{l+1} &= \text{MLP}(\text{BN}(z^l)) + z^l, \end{aligned} \quad (2)$$

where z^{l-1} denotes the output features of the last attention layer, $\text{BN}(\cdot)$, $\text{MHSA}(\cdot)$, and $\text{MLP}(\cdot)$ denote batch normalization (BN) layers, multi-head self-attention (MHSA), and multilayer perceptron (MLP) blocks, respectively. The spatial attention layer allows the model to emphasize relevant spatial information and effectively capture the complex relationships among different facial parts.

In the temporal node attention layer, the computation process is similar, but we apply MHSA to each graph node across all frames within a compact sliding window, which enables the model to focus on temporal dependencies, facilitating the understanding of temporal variations within the sliding window.

3.2.5 Multi-scale spatio-temporal feature learning

Multi-scale learning has shown powerful performance in image processing [45], [53] and video understanding [42], [54]. It is also significant in facial expression analysis since it enables the model to extract both coarse and fine feature representations across different scales, enhancing its ability to capture comprehensive facial structures and temporal dynamics.

For extracting multi-scale temporal features, we use a 1D CNN with stride 2 to achieve temporal downsampling, following ActionFormer [33]. However, for spatial downsampling, applying pooling operations, which are generally used for downsampling images, to graph-structured data presents challenges because it is a type of non-Euclidean structured data. To address this issue, inspired by Xu et al. [55], we introduce FLGP, specifically designed for extracting multi-scale facial graph features. In practice, we design three scales of facial structures. The designed scales and the scale change achieved through FLGP are illustrated in Fig. 4 (b). During each FLGP operation, the facial graph is downsampled by aggregating features from multiple nodes using the max pooling operation.

3.2.6 Model architecture

SpotFormer simultaneously models spatio-temporal relations, as shown in Fig. 4 (a). Specifically, in each spatio-temporal attention block, the model first employs a spatial graph attention layer to model intricate spatial relationships, followed by a temporal node attention layer that captures temporal variations among each graph node across frames. After each spatio-temporal attention block, spatial downsampling and temporal downsampling are performed to aggregate information to generate high-level features. Note that when the facial graph structure is downsampled to one node, subsequent temporal information learning relies solely on temporal node attention layers and temporal downsampling until the temporal resolution is reduced to 1.

3.2.7 Frame-level probability estimation

Finally, after reducing the spatial graph to a single node and temporal information to a single frame through SpotFormer, the remaining single node comprehensively aggregates spatio-temporal information within a compact sliding window. We then use a fully-connected (FC) layer to generate the probability map $p_i = \{p_i^{\text{onset}}, p_i^{\text{apex}}, p_i^{\text{offset}}, p_i^{\text{exp}}, p_i^{\text{norm}}\}$ corresponding to the frame v_i . This map contains the probabilities of v_i being an onset frame, apex frame, offset frame, expression frame, or neutral frame. Additionally, each component in p_i incorporates two probabilities for ME spotting and MaE spotting, respectively. Specifically, $p_i^{\text{onset}} = \{p_i^{\text{mi,onset}}, p_i^{\text{ma,onset}}\}$, $p_i^{\text{apex}} = \{p_i^{\text{mi,apex}}, p_i^{\text{ma,apex}}\}$, $p_i^{\text{offset}} = \{p_i^{\text{mi,offset}}, p_i^{\text{ma,offset}}\}$, $p_i^{\text{exp}} = \{p_i^{\text{mi,exp}}, p_i^{\text{ma,exp}}\}$, $p_i^{\text{norm}} = \{p_i^{\text{mi,norm}}, p_i^{\text{ma,norm}}\}$. The optimization tasks are divided into two binary classification tasks and a three-class classification task for different types of frames, following the optimization method outlined in [23]. Focal-loss [56] is employed to optimize our model, which can be expressed as:

$$\mathcal{L}_{\text{cls}} = - \sum_i y_i \alpha (1 - p_i)^\gamma \log(p_i), \quad (3)$$

where y_i is the ground-truth label, α and γ are hyperparameters, respectively.

3.3 Supervised contrastive learning

We have been focusing on minimizing the divergence between predicted class probabilities and ground-truth class labels so far, potentially overlooking distributional differences among various classes. We notice that distinguishing certain MaEs and MEs near the boundary poses challenges in terms of duration and intensity. Specifically, the annotation of expressions follows the criterion that MaEs are longer than 0.5 seconds, while MEs are below 0.5 seconds. This criterion introduces difficulties in distinguishing expressions whose duration is close to 0.5 seconds. Similar challenges occur when distinguishing between ME frames and neutral frames. This is due to the fact that certain ground-truth MEs exhibit very low intensity, as well as the presence of noise in the optical flow features, causing the misclassification of specific neutral frames as ME frames.

To overcome this issue, we introduce supervised contrastive learning [49] to enhance our model’s discriminative

TABLE 1
Comparison with the state-of-the-art methods on CAS(ME)² and SAMM-LV in terms of F1-score.

Methods	SAMM-LV			CAS(ME) ²			
	MaE	ME	Overall	MaE	ME	Overall	
Traditional methods	MDMD [12]	0.0629	0.0364	0.0445	0.1196	0.0082	0.0376
	Optical Strain [11]	-	-	-	0.1436	0.0098	0.0448
	Zhang et al. [57]	0.0725	0.1331	0.0999	0.2131	0.0547	0.1403
	He [13]	0.4149	0.2162	0.3638	0.3782	0.1965	0.3436
	Zhao et al. [14]	-	-	0.3863	-	-	0.4030
	Wang et al. [58]	0.3724	0.2866	0.3419	0.5061	0.2614	0.4558
Deep-learning methods	Verburg [15]	-	0.0821	-	-	-	-
	LBCNN [59]	-	-	0.0813	-	-	0.0595
	MESNet [16]	-	0.0880	-	-	0.0360	-
	SOFTNet [30]	0.2169	0.1520	0.1881	0.2410	0.1173	0.2022
	3D-CNN [17]	0.1595	0.0466	0.1084	0.2145	0.0714	0.1675
	Concat-CNN [31]	0.3553	0.1155	0.2736	0.2505	0.0153	0.2019
	LSSNet [22]	0.2810	0.1310	0.2380	0.3770	0.0420	0.3250
	MTSN [60]	0.3459	0.0878	0.2867	0.4104	0.0808	0.3620
	ABPN [23]	0.3349	0.1689	0.2908	0.3357	0.1590	0.3117
	AUW-GCN [18]	0.4293	0.1984	0.3728	0.4235	0.1538	0.3834
	LGSNet [19]	-	-	0.3880	-	-	0.4360
	MULT [20]	-	0.2770	-	-	0.1373	-
	Ours	0.4447	0.4281	0.4401	0.5061	0.2817	0.4841

feature learning, aiming to improve its ability to recognize the boundary between different types of expressions. Specifically, we utilize the feature representation before the last classification FC layer as the feature representation for each frame. The supervised contrastive loss is then employed to minimize the distance between feature representations of the same expression class while simultaneously pushing apart feature representations of different expression classes. The expression type label \tilde{y}_i of the frame v_i for the i -th sliding window is used as the supervision information for the supervised contrastive loss. This means that each frame is labeled as a MaE frame, ME frame, or neutral frame. Let I denote a set of samples in a batch, and the loss function can be expressed as:

$$\mathcal{L}_{\text{con}} = \sum_{i \in I} \frac{-1}{|Q(i)|} \sum_{q \in Q(i)} \log \frac{\exp(z_i \cdot z_q / \tau)}{\sum_{e \in E(i)} \exp(z_i \cdot z_e / \tau)}, \quad (4)$$

where $E(i) := I \setminus i$, $Q(i) := \{q \in E(i) \mid \tilde{y}_q = \tilde{y}_i\}$ represents the set of samples in the batch who has the same label with the i -th sample, $\tau \in \mathbb{R}^+$ is a scalar temperature parameter, and z_i is the feature representation of i which is extracted from the network. The overall loss function for the optimization of our model can be formulated as follows:

$$\mathcal{L} = \mathcal{L}_{\text{cls}} + \lambda \mathcal{L}_{\text{con}}, \quad (5)$$

where λ is a weight parameter to balance between classification and supervised contrastive learning.

3.4 Post-processing

Once the series of output probabilities $P = (p_i)_{i=1}^N$ for the entire video V are obtained, we perform MaE spotting and ME spotting independently, following the methodology outlined in [23]. We will elaborate on the ME spotting process, with the MaE spotting process following a similar method. Initially, we spot all potential ME apex frames $U^{\text{mi,apex}}$ based on the criterion $p_l^{\text{mi,apex}} > \theta_{\text{apex}}$, where θ_{apex} is a threshold. For each spotted apex frame $u_l^{\text{mi,apex}} \in U^{\text{mi,apex}}$, we select the onset frame with the highest onset probability from the left side of the apex frame within the

range of $[l - \frac{k^{\text{mi}}}{2}, l - \frac{j^{\text{mi}}}{2}]$. Similarly, we select the offset frame with the highest offset probability from the right side of the apex frame within the range of $[l + \frac{j^{\text{mi}}}{2}, l + \frac{k^{\text{mi}}}{2}]$, where k^{mi} and j^{mi} represent the average duration and minimum duration of a ME, respectively. As a result, a ME proposal ϕ_l is obtained, including the onset frame, offset frame, and expression type. Subsequently, we assign a score $s_l = p_b^{\text{mi,onset}} \times p_l^{\text{mi,apex}} \times p_d^{\text{mi,offset}}$ to ϕ_l , where b and d denote the frame indices of the onset frame and offset frame selected by the aforementioned rule, respectively.

After obtaining all possible expression proposals, we apply non-maximum suppression to eliminate redundant proposals. Specifically, if the overlap rate between two proposals exceeds θ_{overlap} , we compare the assigned scores and discard the proposal with the lower score, thereby obtaining the final spotting results.

4 EXPERIMENTS

In this section, we first introduce the experimental setup (Section 4.1) used in the paper. We then compare our method with state-of-the-art methods to demonstrate the effectiveness of SpotFormer (Section 4.2). Next, we thoroughly evaluate our proposed modules in SpotFormer in the ablation study (Section 4.3). We then investigate the effects from the different designs in SpotFormer (Section 4.4). Finally, we present the detailed expression spotting results and a discussion of the results (Section 4.5).

4.1 Experimental setup

Datasets. We conduct experiments on two datasets: SAMM-LV [61] and CAS(ME)² [62]. The SAMM-LV dataset includes 147 raw long videos with 343 MaE clips and 159 ME clips. The CAS(ME)² dataset includes 87 raw long videos with 300 MaE clips and 57 ME clips. Since the frame rate of the SAMM-LV dataset is 200fps while the frame rate of the CAS(ME)² datasets is 30fps, we subsample every 7th frame from the SAMM dataset to align the frame rates of both datasets.

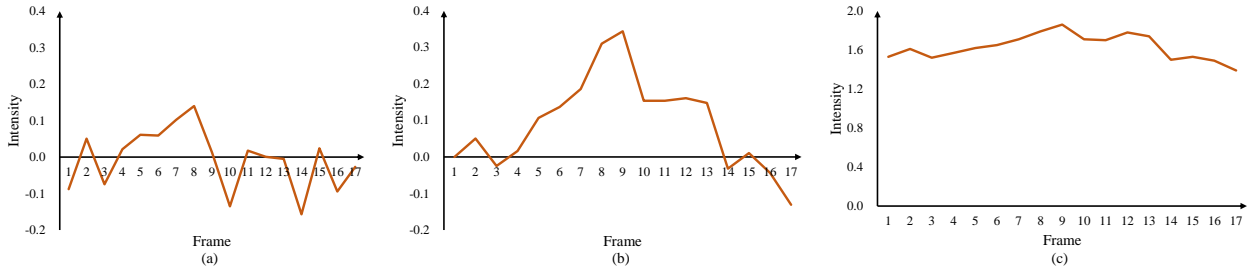


Fig. 5. Some visualization optical flow of certain micro-expression frames computed by three strategies. The data comes from the vertical component of optical flow computed at the left mouth corner when subject 11 from the SAMM-LV dataset is performing a micro-expression. (a) optical flow computed between adjacent frames; (b) optical flow computed using the proposed SW-MRO; (c) optical flow computed with a large sliding window strategy.

Evaluation metric. Following the protocol of MEGC2021, we employ a leave-one-subject-out cross-validation strategy in our experiments. The true positive (TP) is defined based on the Intersection over Union (IoU) between the proposal and the ground-truth expression clip. Specifically, given a ground-truth expression clip and its expression type, we compare it with all expression proposals that have the same estimated expression type. An expression proposal W_{Proposal} , is considered a TP when it satisfies the following condition:

$$\frac{W_{\text{Proposal}} \cap W_{\text{GroundTruth}}}{W_{\text{Proposal}} \cup W_{\text{GroundTruth}}} \geq \theta_{\text{IoU}}, \quad (6)$$

where θ_{IoU} is the IoU threshold, set to 0.5, and $W_{\text{GroundTruth}}$ represents the ground-truth expression proposal (from the onset frame to the offset frame). Otherwise, the proposed expression proposal is considered a false positive (FP). A ground-truth expression clip is counted as a false negative (FN) when it does not match any expression proposal. Note that each ground-truth expression clip corresponds to at most one TP. We calculate the precision rate, recall rate, and F1 score to evaluate the performance of our model and compare it with other methods.

Training details. We use the AdamW optimizer [63] to optimize our model, setting the learning rate to 0.0002, β_1 to 0.7, and β_2 to 0.9. The temperature parameter τ in (4) is set to 0.5. We train our model for 100 epochs with a batch size of 512.

4.2 Comparison with state-of-the-art methods

We first compare our method with the state-of-the-art methods on the SAMM-LV and CAS(ME)² datasets, and the results are shown in Table 1. We report the F1-score for MaE spotting, ME spotting, and overall performance. For the overall performance, our method achieves F1-scores of 0.4401 on the SAMM-LV dataset and 0.4841 on the CAS(ME)² dataset, which outperforms other state-of-the-art methods by 13.4% and 6.2%, respectively. For the MaE spotting, our method achieves an improvement of 3.6% on the SAMM-LV dataset compared to other methods. It is important to emphasize our method’s remarkable effectiveness in ME spotting. The results demonstrate a substantial enhancement with an 49.4% improvement on the SAMM-LV dataset and a 7.8% improvement on the CAS(ME)² dataset

TABLE 2
Results of the ablation study on the effectiveness of the proposed modules.

		SAMM-LV			CAS(ME) ²		
SW-MRO	FLGP	MaE	ME	Overall	MaE	ME	Overall
✗	✗	0.4062	0.2424	0.3687	0.4441	0.0625	0.4105
✗	✓	0.4196	0.2530	0.3760	0.4431	0.0936	0.4113
✓	✗	0.4418	0.3889	0.4274	0.4907	0.2462	0.4684
✓	✓	0.4447	0.4281	0.4401	0.5061	0.2817	0.4841

compared to other state-of-the-art methods. The results show our method’s ability to capture subtle motions that exist in MEs and alleviate the impact of irrelevant motions.

4.3 Ablation studies

We conduct ablation studies to evaluate our proposed modules and Table 2 shows the experimental results. The acronyms **SW-MRO** and **FLGP** denote specific modules in our model. Specifically, **SW-MRO** involves calculating sliding window-based multi-resolution optical flow features instead of optical flow between adjacent frames, while **FLGP** integrates facial local graph pooling operation into SpotFormer for multi-scale spatial feature learning instead of global average pooling over facial graphs. The results show the effectiveness of each proposed module. Notably, the introduction of the SW-MRO enhances the extracted motion features, particularly in revealing subtle motions that exist in MEs. This enhancement leads to a significant overall performance improvement of 17.0%/17.7% on the SAMM-LV and CAS(ME)² datasets. Especially in ME recognition, it has led to an improvement of 69.2%/200.1% on the SAMM-LV and CAS(ME)² datasets. The introduction of facial local graph pooling operation for multi-scale spatial feature learning results in a further improvement of 3.0%/3.4% on the SAMM-LV and CAS(ME)² datasets compared to using global average pooling. This demonstrates the superior representational capabilities of our proposed model.

Fig. 5 shows the qualitative comparison between different optical flow extraction strategies. When computing optical flow between adjacent frames, the motions present in MEs are so subtle that the noise in the optical flow could overshadow these subtle movements, impacting the quality of the data and making it difficult to reveal these

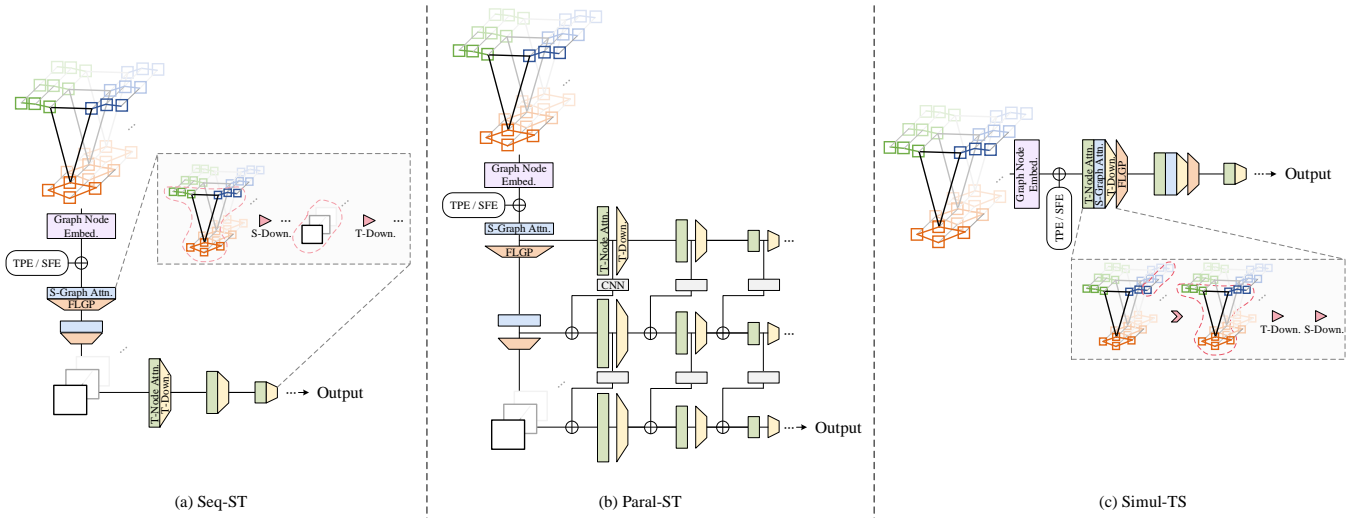


Fig. 6. Overview of the variants of the proposed model architectures. (a) *Seq-ST* encodes each graph and then models temporal variations; (b) *Paral-ST* learns temporal variations in various graph scales and performs multi-scale feature fusion; (c) *Simul-TS* learns temporal variations first and then learns spatial relations simultaneously.

subtle expressions. On the other hand, employing a large sliding window strategy for optical flow computation introduces substantial interference from irrelevant motions such as head movements, posing challenges in accurately detecting facial expressions. On the contrary, the utilization of the SW-MRO helps alleviate these problems. It achieves a balance between amplifying subtle facial muscle motions and mitigating the impact of head movements.

4.4 Model variations

4.4.1 Multiple model architectures

To verify the effectiveness of the SpotFormer, we created multiple model architectures that consider multi-scale spatio-temporal feature learning differently as variants of SpotFormer and then conducted a comprehensive comparison among them. Here, the original architecture of SpotFormer is called *Simul-ST* for clarity since it simultaneously models spatio-temporal relations and enables the comprehensive capture of both spatial and temporal information. The architectures of variants are described as follows:

Seq-ST. This model sequentially learns spatial features first, followed by temporal features. As shown in Fig. 6 (a), we first employ two spatial graph attention layers, each followed by an FLGP layer. After downsampling the facial graph structure to one node, we add temporal node attention layers, where each is followed by a temporal downsampling layer until temporal resolution is downsampled to 1. *Seq-ST* is similar to a general TAL architecture, which encodes spatial information into a feature vector and then learns temporal information to detect potential action instances. In both TAL and FES, temporal information is vital for detecting action instances; such a model can initially focus on spatial details, capturing fine-grained information, and then capturing temporal dynamics.

Paral-ST. Considering that *Seq-ST* lacks the consideration of temporal information in lower graph scales, *Paral-ST* parallelizes temporal learning across different spatial scales

and fuses them. Specifically, as described in Fig. 6 (b), we perform temporal node attention and temporal downsampling operations at each facial graph scale. At each temporal scale, we fuse temporal features from different graph scales by incorporating the output of the temporal node attention layer into the higher graph scale. The incorporation is achieved through a CNN layer followed by an element-wise addition operation. In *Paral-ST* the independent extraction of temporal dynamics for each spatial graph scale and the multi-scale feature fusion ensure a comprehensive understanding of temporal dynamics.

Simul-TS. Would it be better to prioritize temporal node attention first? With such consideration, *Simul-TS* begins with a focus on temporal dynamics and gradually introduces spatial information. As described in Fig. 6 (c), in each attention block, we first perform temporal node attention, followed by spatial graph attention. Subsequently, we perform temporal downsampling and spatial downsampling to generate high-level features. By learning spatial information later in the process, *Simul-TS* treats spatial information as more important.

We validate and compare our proposed multiple multi-scale spatio-temporal model architectures on the SAMM and CAS(ME)² datasets, and the experimental results are shown in Table 3. With the exception of *Paral-ST*, our models use the same number of parameters for a fair comparison.

The results indicate that SpotFormer (*Simul-ST*) achieves the best overall performance, as it learns spatial and temporal information simultaneously. *Seq-ST* is similar to a TAL model, encoding spatial information into a feature vector and then learning temporal information. The comparison results show that simultaneously learning spatio-temporal information better models the spatio-temporal relationships, leading to improved performance. *Paral-ST* (*no more parameter*) considers multi-scale feature fusion without adding additional parameters, we implement it by removing additional CNN layers and using weight-sharing temporal node

TABLE 3
Comparison of multiple model architectures on SAMM-LV and CAS(ME)².

Model	SAMM-LV			CAS(ME) ²			
	MaE	ME	Overall	MaE	ME	Overall	Overall
SpotFormer (Simul-ST)	0.4447	0.4281	0.4401	0.5061	0.2817	0.4841	0.4584
Seq-ST	0.4680	0.3630	0.4367	0.4922	0.2133	0.4630	0.4478
Paral-ST	0.4235	0.3919	0.4139	0.5368	0.2353	0.5054	0.4506
Paral-ST (no addi. para.)	0.4163	0.3378	0.3964	0.5170	0.0984	0.4794	0.4324
Simul-TS	0.4459	0.3959	0.4321	0.4992	0.2121	0.4733	0.4489

TABLE 4
Comparison of different temporal window sizes (receptive fields) on SAMM-LV.

Window Size / Receptive Field	MaE	ME	F1-Score
9	0.4278	0.2419	0.3794
11	0.4272	0.2709	0.3874
15	0.4254	0.3883	0.4151
17	0.4447	0.4281	0.4401
19	0.4397	0.3922	0.4269
21	0.4557	0.3851	0.4350
25	0.4421	0.3408	0.4127

TABLE 5
Results of the ablation study on supervised contrastive learning and the choice of hyperparameter.

λ	SAMM-LV			CAS(ME) ²		
	MaE	ME	Overall	MaE	ME	Overall
0.0	0.4320	0.384	0.4153	0.4495	0.2632	0.4164
0.001	0.4514	0.3704	0.4240	0.4934	0.2716	0.4698
0.003	0.4429	0.3873	0.4261	0.4947	0.2500	0.4704
0.005	0.4447	0.4281	0.4401	0.5061	0.2817	0.4841
0.008	0.4501	0.3881	0.4330	0.4954	0.2029	0.4675
0.01	0.4509	0.3505	0.4230	0.5057	0.1875	0.4758
0.03	0.4345	0.2621	0.3961	0.5024	0.0678	0.4651
0.05	0.4363	0.2723	0.3983	0.4977	0.0345	0.4596

attention layers at each temporal scale. However, the performance of *Paral-ST (no more parameter)* is worse, especially in ME spotting. This is because redundant information is fed into the high-scale branch without being learned properly, thus harmful for expression spotting. *Paral-ST*, with added parameters for processing the lower-scale features, increases the model’s ability to handle multi-scale features. The results of *Simul-TS* indicate that modeling spatial correlations first is better than modeling temporal variations first. This is because, unlike facial expression recognition, where we can first learn temporal information and then learn spatial information (AUs combination) to recognize the exact emotion type, facial expression spotting focuses on detecting the existing facial expressions, making temporal information more crucial.

4.4.2 Temporal window size

We further explore how much temporal information is needed to accurately evaluate one frame. Specifically, we compare different temporal window sizes (i.e., temporal receptive field) for the SW-MRO on the SAMM-LV dataset, and the experimental results are presented in Table 4. The results indicate that the optimal performance is obtained when the temporal window size is set to 17, which demonstrates the effectiveness of our core idea: perceiving complete MEs and distinguishing between MaEs and MEs.

Specifically, the temporal boundary for distinguishing MaEs and MEs is 0.5 seconds, which corresponds to 15 frames when the frame rate is set to 30fps. A receptive field of 17 frames proves sufficient to perceive a complete ME and amplify the motion information that exists in MEs. When the model can accurately spot MEs, windows that exhibit greater intensity of motion, or windows that exhibit a continuous expression and are hard to perceive a trend of this expression occurring or ceasing within a short period, are more likely to contain MaEs.

Based on this idea, the model can capture the temporal variations necessary to distinguish between general MaEs and MEs. A smaller window size cannot provide sufficient temporal information, while an increase in the window size results in more frames, potentially leading to information redundancy and increased ambiguity in distinguishing between MaEs and MEs. Moreover, larger temporal window sizes may cause more severe head movement problems, negatively impacting overall performance.

4.4.3 Supervised contrastive loss and hyperparameter λ

Table 5 shows the experimental results of introducing supervised contrastive learning into our model and the impact of the hyperparameter λ in (5), which is set to balance classification and supervised contrastive learning. We observe that the introduction of the supervised contrastive loss enables our model to better recognize the boundaries distinguishing between different types of expressions, resulting in an improvement of 6.0%/16.3% on the SAMM-LV and CAS(ME)² datasets. The optimal value for λ is 0.005, increasing λ beyond this value starts to impact standard classification, leading to a decrease in spotting accuracy.

Fig. 7 shows the qualitative comparison between scenarios with and without supervised contrastive learning. In the inference phase, we randomly sampled frames and applied principal component analysis (PCA) [64] to analyze the distribution of various expression classes. Subsequently, we marked each frame with its corresponding ground-truth expression label. In Fig. 7 (a) and (b), we examine the PCA distribution of specific MaE frames and ME frames with and without supervised contrastive learning. Moving to Fig. 7 (c) and (d), we compare the PCA distribution of specific neutral frames and ME frames with and without supervised contrastive learning. The results indicate that, in the absence of supervised contrastive learning, our model may face challenges distinguishing certain MaE frames from ME frames due to subtle differences. This leads to mixed distributions and misclassification. Additionally, neutral frames may be mistakenly classified as ME frames, as optical flow noise introduces slight differences that the model treats as ME motion information, resulting in incorrect ME proposals

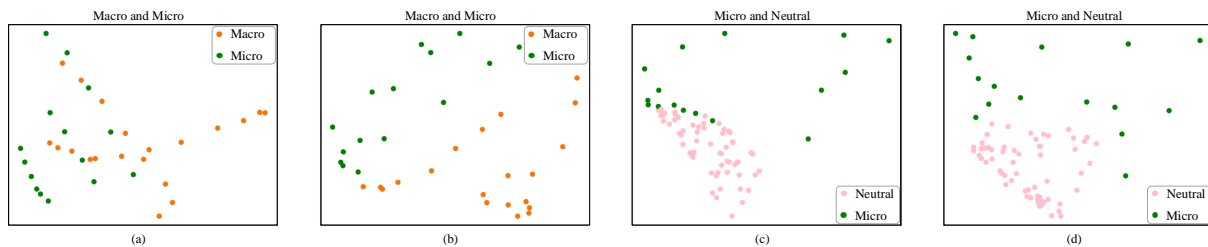


Fig. 7. Visualization analysis of supervised contrastive learning. (a) and (b) show the PCA distribution of certain macro- and micro-expression frames: (a) without supervised contrastive learning and (b) with supervised contrastive learning. (c) and (d) depict the PCA distribution of certain micro-expression frames and neutral frames: (c) without supervised contrastive learning and (d) with supervised contrastive learning.

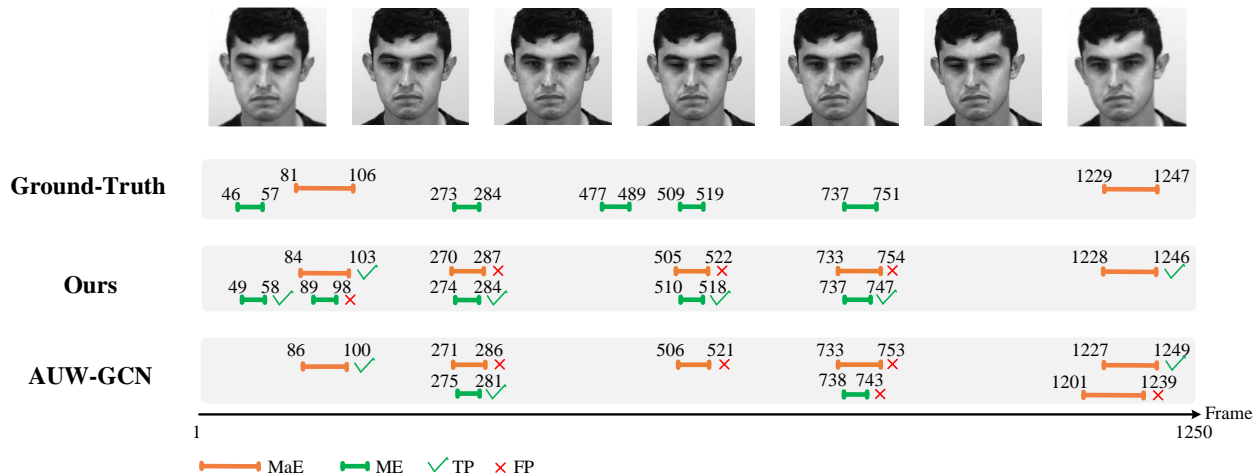


Fig. 8. Qualitative results of our method on SAMM-LV. The example video is “006_1”, whose frame rate has been downsampled to 30fps.

TABLE 6
Detailed spotting results of the proposed method on SAMM-LV and CAS(ME)².

Dataset	SAMM-LV			CAS(ME) ²		
	MaE	ME	Overall	MaE	ME	Overall
Total	343	159	502	300	57	357
TP	163	61	224	165	10	175
FP	227	65	292	187	4	191
FN	180	98	278	135	47	182
Precision	0.4179	0.4841	0.4341	0.4688	0.7143	0.4781
Recall	0.4752	0.3836	0.4462	0.5500	0.1754	0.4902
F1-Score	0.4447	0.4281	0.4401	0.5061	0.2817	0.4841

detection. With the introduction of supervised contrastive learning into our model, the domain discrepancy increases, thus significantly improving the accuracy of expression recognition.

4.5 Detailed results

Table 6 shows the detailed results on the SAMM-LV and CAS(ME)² datasets. Our method achieves a recall rate of approximately 0.5 in MaE spotting and 0.4 in ME spotting. The exception is for ME spotting on the CAS(ME)² dataset. The results indicate that it achieves a high precision score while a low recall score, which may be due to several factors. One primary reason is the scarcity of ME data and data imbalance in the CAS(ME)² dataset, which only contains 57 ME clips, some of which involve only eye blinking—considered

irrelevant motions for facial expression spotting. Furthermore, owing to our model’s strong discriminatory capability and the incorporation of supervised contrastive learning, the model cautiously evaluates ME frames based on limited data. Consequently, it achieves a high precision rate but a low recall rate.

Fig. 8 shows qualitative results on an example video, showcasing both ground-truth expression intervals and detected expression proposals to demonstrate the effectiveness of our model.

5 CONCLUSION

In this paper, we proposed an efficient framework for FES. First, we proposed a SW-MRO feature to magnify motion information while alleviating severe head movement issues.

Such an optical flow feature is designed to perceive complete MEs and discern the differences between MaEs and MEs. Then, we presented SpotFormer, a powerful graph-based Transformer designed to learn multi-scale spatio-temporal relationships from SW-MRO features for frame-level probability estimation. In SpotFormer, we proposed FLGP operations for downsampling facial graph-structured data to achieve multi-scale spatial feature fusion. In addition, we introduced supervised contrastive learning into SpotFormer to enhance the discriminability between different types of expressions. Extensive comparative experiments and ablation studies on SAMM-LV and CAS(ME)² demonstrated the effectiveness of our proposed framework, particularly in ME spotting.

Our model also has some limitations. Performance under conditions with fewer available MEs requires improvement, as evidenced by the experimental results on the CAS(ME)² dataset. Although our optical flow extraction using receptive field adaptive sliding window strategy is effective in extracting robust motion features, it is still not computationally friendly. In future work, we aim to explore a more efficient method for extracting robust motion features and develop an end-to-end framework for FES.

ACKNOWLEDGMENTS

This work was partially supported by Innovation Platform for Society 5.0 from Japan Ministry of Education, Culture, Sports, Science and Technology, and JSPS KAKENHI Grant Number JP24K03010.

REFERENCES

- [1] P. Ekman, "Emotions revealed: Recognizing faces and feelings to improve communication and emotional life," *Holt Paperback*, vol. 128, no. 8, pp. 140–140, 2003.
- [2] C. A. Corneanu, M. O. Simón, J. F. Cohn, and S. E. Guerrero, "Survey on RGB, 3D, thermal, and multimodal approaches for facial expression recognition: History, trends, and affect-related applications," *IEEE Transactions on Pattern Analysis and Machine Intelligence*, vol. 38, no. 8, pp. 1548–1568, 2016.
- [3] T. Fukuda, J. Taguri, F. Arai, M. Nakashima, D. Tachibana, and Y. Hasegawa, "Facial expression of robot face for human-robot mutual communication," in *Proceedings of the International Conference on Robotics and Automation*, vol. 1. IEEE, 2002, pp. 46–51.
- [4] B. A. Kopper and D. L. Epperson, "The experience and expression of anger: Relationships with gender, gender role socialization, depression, and mental health functioning," *Journal of Counseling Psychology*, vol. 43, no. 2, p. 158, 1996.
- [5] J. Thies, M. Zollhöfer, M. Stamminger, C. Theobalt, and M. Nießner, "FaceVR: Real-time gaze-aware facial reenactment in virtual reality," *ACM Transactions on Graphics*, vol. 37, no. 2, pp. 1–15, 2018.
- [6] W.-J. Yan, Q. Wu, J. Liang, Y.-H. Chen, and X. Fu, "How fast are the leaked facial expressions: The duration of micro-expressions," *Journal of Nonverbal Behavior*, vol. 37, pp. 217–230, 2013.
- [7] B. Bhushan, "Study of facial micro-expressions in psychology," *Understanding Facial Expressions in Communication: Cross-cultural and Multidisciplinary Perspectives*, pp. 265–286, 2015.
- [8] P. Ekman, *Telling lies: Clues to deceit in the marketplace, politics, and marriage (revised edition)*. WW Norton & Company, 2009.
- [9] J. Endres and A. Laidlaw, "Micro-expression recognition training in medical students: a pilot study," *BMC Medical Education*, vol. 9, no. 1, pp. 1–6, 2009.
- [10] M. O'sullivan, M. G. Frank, C. M. Hurley, and J. Tiwana, "Police lie detection accuracy: The effect of lie scenario." *Law and Human Behavior*, vol. 33, no. 6, p. 530, 2009.
- [11] Y. Gan, S. Liong, D. Zheng, S. Li, and C. Bin, "Optical strain based macro-and micro-expression sequence spotting in long video," in *Proceedings of the International Conference on Automatic Face and Gesture Recognition*. IEEE, 2020.
- [12] Y. He, S.-J. Wang, J. Li, and M. H. Yap, "Spotting macro-and micro-expression intervals in long video sequences," in *Proceedings of the International Conference on Automatic Face and Gesture Recognition*. IEEE, 2020, pp. 742–748.
- [13] H. Yuhong, "Research on micro-expression spotting method based on optical flow features," in *Proceedings of the International Conference on Multimedia*. ACM, 2021, pp. 4803–4807.
- [14] Y. Zhao, X. Tong, Z. Zhu, J. Sheng, L. Dai, L. Xu, X. Xia, Y. Jiang, and J. Li, "Rethinking optical flow methods for micro-expression spotting," in *Proceedings of the International Conference on Multimedia*. ACM, 2022, pp. 7175–7179.
- [15] M. Verburg and V. Menkovski, "Micro-expression detection in long videos using optical flow and recurrent neural networks," in *Proceedings of the International Conference on Automatic Face and Gesture Recognition*. IEEE, 2019, pp. 1–6.
- [16] S.-J. Wang, Y. He, J. Li, and X. Fu, "MESNet: A convolutional neural network for spotting multi-scale micro-expression intervals in long videos," *IEEE Transactions on Image Processing*, vol. 30, pp. 3956–3969, 2021.
- [17] C. H. Yap, M. H. Yap, A. Davison, C. Kendrick, J. Li, S.-J. Wang, and R. Cunningham, "3D-CNN for facial micro-and macro-expression spotting on long video sequences using temporal oriented reference frame," in *Proceedings of the International Conference on Multimedia*. ACM, 2022, pp. 7016–7020.
- [18] S. Yin, S. Wu, T. Xu, S. Liu, S. Zhao, and E. Chen, "AU-aware graph convolutional network for macroand micro-expression spotting," in *Proceedings of the International Conference on Multimedia and Expo*. IEEE, 2023, pp. 228–233.
- [19] W.-W. Yu, J. Jiang, K.-F. Yang, H.-M. Yan, and Y.-J. Li, "LGSNet: A two-stream network for micro- and macro-expression spotting with background modeling," *IEEE Transactions on Affective Computing*, pp. 1–18, 2023.
- [20] X. Guo, X. Zhang, L. Li, and Z. Xia, "Micro-expression spotting with multi-scale local transformer in long videos," *Pattern Recognition Letters*, vol. 168, pp. 146–152, 2023.
- [21] Y. Guo, B. Li, X. Ben, Y. Ren, J. Zhang, R. Yan, and Y. Li, "A magnitude and angle combined optical flow feature for microexpression spotting," *IEEE MultiMedia*, vol. 28, no. 2, pp. 29–39, 2021.
- [22] W.-W. Yu, J. Jiang, and Y.-J. Li, "LSSNet: A two-stream convolutional neural network for spotting macro-and micro-expression in long videos," in *Proceedings of the International Conference on Multimedia*. ACM, 2021, pp. 4745–4749.
- [23] W. Leng, S. Zhao, Y. Zhang, S. Liu, X. Mao, H. Wang, T. Xu, and E. Chen, "Abpn: Apex and boundary perception network for micro-and macro-expression spotting," in *Proceedings of the International Conference on Multimedia*. ACM, 2022, pp. 7160–7164.
- [24] J. Carreira and A. Zisserman, "Quo vadis, action recognition? a new model and the kinetics dataset," in *Proceedings of the Conference on Computer Vision and Pattern Recognition*. IEEE, 2017, pp. 6299–6308.
- [25] Y. Deng, H. Hayashi, and H. Nagahara, "Multi-scale spatio-temporal graph convolutional network for facial expression spotting," in *Proceedings of the International Conference on Automatic Face and Gesture Recognition*. IEEE, 2024.
- [26] A. Moilanen, G. Zhao, and M. Pietikäinen, "Spotting rapid facial movements from videos using appearance-based feature difference analysis," in *Proceedings of the International Conference on Pattern Recognition*. IEEE, 2014, pp. 1722–1727.
- [27] A. K. Davison, M. H. Yap, and C. Lansley, "Micro-facial movement detection using individualised baselines and histogram-based descriptors," in *Proceedings of the International Conference on Systems, Man, and Cybernetics*. IEEE, 2015, pp. 1864–1869.
- [28] S.-J. Wang, S. Wu, X. Qian, J. Li, and X. Fu, "A main directional maximal difference analysis for spotting facial movements from long-term videos," *Neurocomputing*, vol. 230, pp. 382–389, 2017.
- [29] Z. Zhang, T. Chen, H. Meng, G. Liu, and X. Fu, "SMEConvNet: A convolutional neural network for spotting spontaneous facial micro-expression from long videos," *IEEE Access*, vol. 6, pp. 71 143–71 151, 2018.
- [30] G.-B. Liong, J. See, and L.-K. Wong, "Shallow optical flow three-stream cnn for macro-and micro-expression spotting from long videos," in *Proceedings of the International Conference on Image Processing*. IEEE, 2021, pp. 2643–2647.

- [31] B. Yang, J. Wu, Z. Zhou, M. Komiya, K. Kishimoto, J. Xu, K. Nonaka, T. Horiuchi, S. Komorita, G. Hattori *et al.*, "Facial action unit-based deep learning framework for spotting macro- and micro-expressions in long video sequences," in *Proceedings of the International Conference on Multimedia*. ACM, 2021, pp. 4794–4798.
- [32] Y.-J. Liu, J.-K. Zhang, W.-J. Yan, S.-J. Wang, G. Zhao, and X. Fu, "A main directional mean optical flow feature for spontaneous micro-expression recognition," *IEEE Transactions on Affective Computing*, vol. 7, no. 4, pp. 299–310, 2015.
- [33] C.-L. Zhang, J. Wu, and Y. Li, "Actionformer: Localizing moments of actions with transformers," in *Proceedings of the European Conference on Computer Vision*. Springer, 2022, pp. 492–510.
- [34] L. Yang, H. Peng, D. Zhang, J. Fu, and J. Han, "Revisiting anchor mechanisms for temporal action localization," *IEEE Transactions on Image Processing*, vol. 29, pp. 8535–8548, 2020.
- [35] H. Xu, A. Das, and K. Saenko, "R-c3d: Region convolutional 3d network for temporal activity detection," in *Proceedings of the International Conference on Computer Vision (ICCV)*. IEEE, Oct 2017.
- [36] Y.-W. Chao, S. Vijayanarasimhan, B. Seybold, D. A. Ross, J. Deng, and R. Sukthankar, "Rethinking the faster r-cnn architecture for temporal action localization," in *Proceedings of the Conference on Computer Vision and Pattern Recognition*. IEEE, June 2018.
- [37] T. Lin, X. Zhao, H. Su, C. Wang, and M. Yang, "Bsn: Boundary sensitive network for temporal action proposal generation," in *Proceedings of the European Conference on Computer Vision*. Springer, September 2018.
- [38] T. Lin, X. Liu, X. Li, E. Ding, and S. Wen, "Bmn: Boundary-matching network for temporal action proposal generation," in *Proceedings of the International Conference on Computer Vision*. IEEE/CVF, October 2019.
- [39] P. Zhao, L. Xie, C. Ju, Y. Zhang, Y. Wang, and Q. Tian, "Bottom-up temporal action localization with mutual regularization," in *Proceedings of the European Conference on Computer Vision*. Springer, 2020, pp. 539–555.
- [40] Z. Zhu, W. Tang, L. Wang, N. Zheng, and G. Hua, "Enriching local and global contexts for temporal action localization," in *Proceedings of the International Conference on Computer Vision*. IEEE/CVF, October 2021, pp. 13 516–13 525.
- [41] S. Nag, X. Zhu, Y.-Z. Song, and T. Xiang, "Post-processing temporal action detection," in *Proceedings of the Conference on Computer Vision and Pattern Recognition*. IEEE/CVF, June 2023, pp. 18 837–18 845.
- [42] J. Shao, X. Wang, R. Quan, J. Zheng, J. Yang, and Y. Yang, "Action sensitivity learning for temporal action localization," in *Proceedings of the International Conference on Computer Vision*. IEEE/CVF, October 2023, pp. 13 457–13 469.
- [43] A. Vaswani, N. Shazeer, N. Parmar, J. Uszkoreit, L. Jones, A. N. Gomez, L. Kaiser, and I. Polosukhin, "Attention is all you need," in *Proceedings of the International Conference on Neural Information Processing Systems*. Curran Associates Inc., 2017, p. 6000–6010.
- [44] A. Dosovitskiy, L. Beyer, A. Kolesnikov, D. Weissenborn, X. Zhai, T. Unterthiner, M. Dehghani, M. Minderer, G. Heigold, S. Gelly, J. Uszkoreit, and N. Houlsby, "An image is worth 16x16 words: Transformers for image recognition at scale," in *Proceedings of the International Conference on Learning Representations*, 2021.
- [45] Z. Liu, Y. Lin, Y. Cao, H. Hu, Y. Wei, Z. Zhang, S. Lin, and B. Guo, "Swin transformer: Hierarchical vision transformer using shifted windows," in *Proceedings of the International Conference on Computer Vision*. IEEE/CVF, 2021, pp. 10 012–10 022.
- [46] A. Arnab, M. Dehghani, G. Heigold, C. Sun, M. Lučić, and C. Schmid, "ViVit: A video vision transformer," in *Proceedings of the International Conference on Computer Vision*. IEEE/CVF, October 2021, pp. 6836–6846.
- [47] Z. Liu, J. Ning, Y. Cao, Y. Wei, Z. Zhang, S. Lin, and H. Hu, "Video swin transformer," in *Proceedings of the Conference on Computer Vision and Pattern Recognition*. IEEE/CVF, June 2022, pp. 3202–3211.
- [48] T. Chen, S. Kornblith, M. Norouzi, and G. Hinton, "A simple framework for contrastive learning of visual representations," in *Proceedings of the International Conference on Machine Learning*. PMLR, 2020, pp. 1597–1607.
- [49] P. Khosla, P. Teterwak, C. Wang, A. Sarna, Y. Tian, P. Isola, A. Maschinot, C. Liu, and D. Krishnan, "Supervised contrastive learning," in *Proceedings of the Advances in Neural Information Processing Systems*, vol. 33, 2020, pp. 18 661–18 673.
- [50] C. Chen, "PyTorch Face Landmark: A fast and accurate facial landmark detector," 2021. [Online]. Available: https://github.com/cunjian/pytorch_face_landmark
- [51] G. Farneback, "Two-frame motion estimation based on polynomial expansion," in *Proceedings of the Scandinavian Conference on Image Analysis*. Springer, 2003, pp. 363–370.
- [52] Y. Zhang, B. Wu, W. Li, L. Duan, and C. Gan, "STST: Spatial-temporal specialized transformer for skeleton-based action recognition," in *Proceedings of the International Conference on Multimedia*. ACM, 2021, p. 3229–3237.
- [53] T.-Y. Lin, P. Dollár, R. Girshick, K. He, B. Hariharan, and S. Belongie, "Feature pyramid networks for object detection," in *Proceedings of the Conference on Computer Vision and Pattern Recognition*. IEEE/CVF, 2017, pp. 2117–2125.
- [54] H. Fan, B. Xiong, K. Mangalam, Y. Li, Z. Yan, J. Malik, and C. Feichtenhofer, "Multiscale vision transformers," in *Proceedings of the International Conference on Computer Vision*. IEEE/CVF, October 2021, pp. 6824–6835.
- [55] T. Xu and W. Takano, "Graph stacked hourglass networks for 3D human pose estimation," in *Proceedings of the Conference on Computer Vision and Pattern Recognition*. IEEE/CVF, 2021, pp. 16 105–16 114.
- [56] T.-Y. Lin, P. Goyal, R. Girshick, K. He, and P. Dollár, "Focal loss for dense object detection," in *Proceedings of the International Conference on Computer Vision*. IEEE/CVF, 2017, pp. 2980–2988.
- [57] L.-W. Zhang, J. Li, S.-J. Wang, X.-H. Duan, W.-J. Yan, H.-Y. Xie, and S.-C. Huang, "Spatio-temporal fusion for macro- and micro-expression spotting in long video sequences," in *Proceedings of the International Conference on Automatic Face and Gesture Recognition*. IEEE, 2020, pp. 734–741.
- [58] J. Wang, S. Xu, and T. Zhang, "A unique M-pattern for micro-expression spotting in long videos," in *Proceedings of the International Conference on Learning Representations*, 2024.
- [59] H. Pan, L. Xie, and Z. Wang, "Local bilinear convolutional neural network for spotting macro- and micro-expression intervals in long video sequences," in *Proceedings of the International Conference on Automatic Face and Gesture Recognition*. IEEE, 2020, pp. 749–753.
- [60] G. B. Liong, S.-T. Liong, J. See, and C.-S. Chan, "MTSN: A multi-temporal stream network for spotting facial macro- and micro-expression with hard and soft pseudo-labels," in *Proceedings of the Workshop on Facial Micro-Expression: Advanced Techniques for Multimodal Facial Expression Analysis*. ACM, 2022, pp. 3–10.
- [61] C. H. Yap, C. Kendrick, and M. H. Yap, "Samm long videos: A spontaneous facial micro- and macro-expressions dataset," in *Proceedings of the International Conference on Automatic Face and Gesture Recognition*. IEEE, 2020, pp. 771–776.
- [62] F. Qu, S.-J. Wang, W.-J. Yan, H. Li, S. Wu, and X. Fu, "CAS(ME)²: A database for spontaneous macro-expression and micro-expression spotting and recognition," *IEEE Transactions on Affective Computing*, vol. 9, no. 4, pp. 424–436, 2017.
- [63] I. Loshchilov and F. Hutter, "Decoupled weight decay regularization," in *Proceedings of the International Conference on Learning Representations*, 2019.
- [64] R. Bro and A. K. Smilde, "Principal component analysis," *Analytical Methods*, vol. 6, no. 9, pp. 2812–2831, 2014.



Yicheng Deng received the B.Eng. and M.Eng. degrees from Beijing Jiaotong University, Beijing, China, in 2019 and 2022, respectively. He is now pursuing his Ph.D. degree in Osaka University. His research interests include facial expression analysis and video understanding.



Hideaki Hayashi (S' 13–M' 16) received the B.E., M.Eng, and D.Eng. degrees from Hiroshima University, Hiroshima, Japan, in 2012, 2014, and 2016 respectively. He was a Research Fellow of the Japan Society for the Promotion of Science from 2015 to 2017 and an assistant professor in Department of Advanced Information Technology, Kyushu University from 2017 to 2022. He is currently an associate professor with Institute for Datability Science, Osaka University. His research interests focus on neural networks,

machine learning, and medical data analysis.



Hajime Nagahara is a professor at Institute for Datability Science, Osaka University, since 2017. He received Ph.D. degree in system engineering from Osaka University in 2001. He was a research associate of the Japan Society for the Promotion of Science from 2001 to 2003. He was an assistant professor at the Graduate School of Engineering Science, Osaka University, Japan from 2003 to 2010. He was an associate professor in Faculty of information science and electrical engineering at Kyushu University

from 2010 to 2017. He was a visiting associate professor at CREA University of Picardie Jules Verns, France, in 2005. He was a visiting researcher at Columbia University in 2007-2008 and 2016-2017. Computational photography and computer vision are his research areas. He received an ACM VRST2003 Honorable Mention Award in 2003, IPSJ Nagao Special Researcher Award in 2012, ICCP2016 Best Paper Runners-up, and SSII Takagi Award in 2016. He is a program chair in ICCP2019, Associate Editor for IEEE Transaction on Computational Imaging in 2019-2022, and Director of Information Processing Society of Japan in 2022-2024.